Published in final edited form as:

J Chem Theory Comput. 2020 January 14; 16(1): 587–600. doi:10.1021/acs.jctc.9b00823.

Benchmarking the performance of time-dependent density functional theory methods on biochromophores

Yihan Shao[†], **Ye Mei**[‡], **Dage Sundholm**[¶], **Ville R. I. Kaila**[§]

[†]Department of Chemistry and Biochemistry, University of Oklahoma, Norman, Oklahoma 73019, USA [‡]State Key Laboratory of Precision Spectroscopy, Institute of Theoretical and Computational Science, East China Normal University, Shanghai 200062, China; NYU-ECNU Center for Computational Chemistry at NYU Shanghai, Shanghai, China 200062; Q-Chem Inc., 6601 Owens Drive, Suite 105, Pleasanton, CA 94588, USA [¶]Department of Chemistry, Faculty of Science, P.O. Box 55, FIN-00014 University of Helsinki, Finland [§]Department Chemie, Technische Universität München (TUM), Lichtenbergstrasse 4, D-85747 Garching, Germany.; Department of Biochemistry and Biophysics, Stockholm University, SE-10691 Stockholm, Sweden

Abstract

Quantum chemical calculations are important for elucidating light-capturing mechanisms in photobiological systems. The time-dependent density functional theory (TDDFT) has become a popular methodology due to its balance between accuracy and computational scaling, despite its problems in describing, *e.g.*, charge transfer states. As a step towards systematically understanding the performance of TDDFT calculations on biomolecular systems, we here study 17 commonly used density functionals, including 7 long-range separated functionals, and compare the obtained results with excitation energies calculated at the approximate second order coupled-cluster theory level (CC2). The benchmarking set includes the first five singlet excited states of 11 chemical analogs of biochromophores from the green fluorescent protein (GFP), rhodopsin/bacteriorhodopsin (Rh/bR), and the photoactive yellow protein (PYP). We find that commonly used pure density functionals such as BP86, PBE, M11-L and hybrid functionals with 20%-25% of Hartree-Fock (HF) exchange (B3LYP, PBE0) have a tendency to consistently underestimating vertical excitation energies (VEE) relative to the CC2 values, whereas hybrid density functionals with around 50% HF exchange such as BHLYP, PBE50 and M06-2X as well as long-range corrected functionals such as CAM-B3LYP, ωPBE, ωPBEh, ωB97X, ωB97XD, BNL, and M11 overestimate the VEEs. We observe that calculations using the CAM-B3LYP and ωPBEh functionals with 65% and 100% long-range HF exchange, respectively, lead to an overestimation of the VEEs by 0.2-0.3 eV for the benchmarking set. To reduce the systematic error, we introduce here two new empirical functionals: CAMh-B3LYP and ωhPBE0, for which we adjusted the long-range HF exchange to 50%. The introduced parameterization reduces the mean signed average (MSA) deviation to 0.07 eV and the root mean square (RMS) deviation to 0.17 eV as compared to the CC2 values. In the present TDDFT calculations using the aug-def2-TZVP basis sets, the best performing functionals relative to CC2 are: ωhPBE0 (RMS=0.17, MSA=0.06 eV); CAMh-B3LYP (RMS=0.16, MSA=0.07 eV); and PBE0 (RMS=0.23, MSA=−0.14 eV). For the the popular range-

yihan.shao@ou.edu; dage.sundholm@helsinki.fi; ville.kaila@ch.tum.de, ville.kaila@dbb.su.se.

separated CAM-B3LYP functional, we obtain a RMS value of 0.31 eV and a MSA value of 0.25 eV, which can be compared with the RMS and MSA values of 0.37 eV and −0.31 eV as obtained at the B3LYP level.

Graphical Abstract

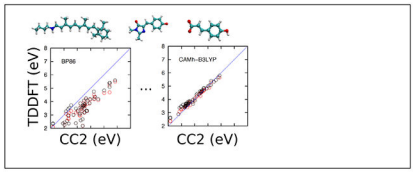

1 Introduction

The development of accurate electronic structure theory methods for studies of electronic excited states has opened new possibilities for elucidating molecular mechanisms of photobiological processes.[1–24] In photobiological studies, the employed computational method should be able to predict optical transitions within chemical accuracy and have a favorable computational scaling that allows modeling of large extended systems of biochromophores embedded by nearby protein residues. Linear-response time-dependent density functional theory (TDDFT) calculations[25–32] provide excitation energies at relatively low computational costs and have therefore become a popular approach for investigating excited states of large molecules. A large number of density functionals have been developed,[33–36] which can be divided into different categories, such as functionals at the local density approximation (LDA), functionals at the generalized gradient approximation (GGA), meta-GGA functionals, hybrid functionals, range-separated functionals, as well as double-hybrid functionals. However, many functionals are known to provide an inadequate description for charge-transfer and Rydberg excitations,[37,38] affecting the accuracy of calculated excitation energies for biomolecules and large molecules.

Correlated *ab initio* methods are generally more accurate. However, the computational scaling renders photobiological applications difficult at correlated *ab initio* levels, because the chromophore and its nearest environment have to be considered at the quantum mechanical (QM) level when aiming at accurate results. Even low-order correlated *ab initio* methods, such as approximate second-order coupled cluster (CC2)[39,40] calculations are computationally expensive for large biochromophores. The computational cost can, however, be enhanced by using the reduced virtual space (RVS) approach[10,14,22,41,42] and algorithms based on Laplace transformations.[43,44] Nevertheless, low-order *ab initio* methods fail to describe excited states when the ground state has a significant multiconfiguration character or double excitations are needed to accurately describe the excited state. The molecular structure and the potential energy surface of the excited states may in such cases be less accurate at the low-order *ab initio* levels than obtained in TDDFT calculations.[45,46]

A number of benchmark studies have reported comparisons of excitation energies calculated using various TDDFT functionals with experimental data and with values obtained at correlated *ab initio* levels.[47–67] Leang *et al.*,[62] studied the performance of 24 density

functionals, including 14 meta-GGA functionals and one range-separated functional on excitation energies for 14 small organic molecules. They found that the M06-2X[68] and PBE0[69] functionals have the smallest mean absolute errors (MAE) of 0.26 eV and 0.28 eV as compared with experimental values, respectively. The CAM-B3LYP range-separated functional[70] was found to have an MAE of about 0.3 eV for singlet excited states, whereas a large MAE of about 1.1 eV was obtained for the excitation energies of excited triplet states.

Isegawa *et al.*[64] reported excitation energies calculated at the TDDFT level using 30 density functionals including many commonly-used meta-GGAs and range-separated functionals. They also reported excitation energies for 69 valence and Rydberg states of 11 small organic molecules. They found that the M06-2X[68] and the ωB97X-D[71] functionals yield the smallest MAE error of 0.30 eV. The use of the CAM-B3LYP functional resulted in a slightly larger MAE error of 0.32 eV.

Charaf-Eddin *et al.*[65] calculated the absorption and emission spectra of 20 conjugated molecules in solvents with six hybrid functionals (B3LYP,[72–74] PBE0,[69] M06,[68] M06-2X,[68] CAM-B3LYP[70] and LC-PBE[75,76]) and found that the B3LYP functional provides the smallest MAE errors for the absorption and emission maxima. They also noticed that the M06-2X functional provides accurate excitation energies for problematic molecules.

Fang *et al.*[66] calculated vertical, adiabatic and 0-0 excitation energies for 96 excited states of 79 organic and inorganic molecules using low-order correlated *ab initio* methods such as configuration interaction singles (CIS) and CC2. They compared the obtained values with excitation energies calculated at the TDDFT level using six functionals (BP86,[77–79] B3LYP, PBE0, M06-2X, M06-HF,[80] CAM-B3LYP, and ωB97X-D). The 0-0 excitation energies obtained at the CC2 level were found to be in the best agreement with experimental values. The B3LYP, PBE0, M06-2X, CAM-B3LYP, and ωB97X-D functionals also yield values that largely agree with experimental data, whereas larger MAE errors were obtained with BP86, M06-HF and CIS.

Here, we employ the biomolecular benchmarking set of Send *et al.*,[57] who performed CC2 calculations and TDDFT calculations using the B3LYP functional on excited states of biochromophore models from retinal proteins, green fluorescent protein (GFP) and the photoactive yellow protein (PYP). They compared the obtained vertical excitation energies (VEE) with benchmarking data calculated at the many-body Green's function theory level by Ma *et al.*[54] Send *et al.* found that the VEEs calculated at the CC2 level for the lowest excited states of GFP and retinal chromophores agreed within 0.15 eV with experimental values, whereas the B3LYP calculations yielded VEEs that had a somewhat larger deviation of 0.1-0.3 eV from the experimental values. For the PYP chromophore models, larger deviations of 0.3-0.4 eV and 0.1-0.5 eV were obtained at the CC2 and B3LYP levels, respectively.

Since these chromophores are particularly relevant for photobiological applications, we extend the TDDFT calculations from B3LYP to 14 other density functionals and to two new empirical functionals. We compare the obtained TDDFT results with previously calculated VEEs at the CC2 level and with experimental data. We address: (I) how range-separated

functionals such as CAM-B3LYP,[70] ωB97X,[81] ωB97X-D,[71] ωPBEh[82] perform relatively to the CC2 method, (II) we investigate the extent of previously reported overestimation of VEEs when using range-separated functionals and address ways to reduce this systematic error, (III) we investigate the performance of the PBE0 and M06-2X functionals on biochromophores, (IV) we estimate errors introduced by the Tamm-Dancoff approximation, and (V) we study ways to accelerate the convergence of the VEEs calculated at the TDDFT level towards the basis set limit.

This article is structured as follows. In Section 2, we briefly review the theory of linear-response time-dependent density functional theory (TDDFT) and introduce the employed functionals. In Section 3, we discuss the overall performance of different TDDFT functionals, and in Section 4 we summarize the obtained results.

2 Computational details

2.1 TDDFT and the Tamm-Dancoff approximation (TDA)

Time-dependent density functional theory can to first order be formulated as linear response to the density functional theory (DFT) calculation on the ground state,

$$\begin{pmatrix} A & B \\ B & A \end{pmatrix} \begin{pmatrix} X \\ Y \end{pmatrix} = \Delta E \begin{pmatrix} 1 & 0 \\ 0 & -1 \end{pmatrix} \begin{pmatrix} X \\ Y \end{pmatrix}. \tag{1}$$

where X and Y are the first-order orbital response and ΔE is the corresponding excitation energy. For the general case of range-separated functionals, the A and B matrices are given by

$$\begin{aligned} A_{ia,\,jb} &= \delta_{ij}\delta_{ab}(\epsilon_a - \epsilon_i) + (ia \mid jb) - C_{\mathrm{HF}}^{\mathrm{sr}}(ij \mid ab)_{sr} - C_{\mathrm{HF}}^{\mathrm{lr}}(ij \mid ab)_{\mathrm{lr}} + (ia \mid \varpi \mid jb) \\ B_{ia,\,jb} &= (ia \mid bj) - C_{\mathrm{HF}}^{\mathrm{sr}}(ib \mid aj)_{\mathrm{sr}} - C_{\mathrm{HF}}^{\mathrm{lr}}(ib \mid aj)_{\mathrm{lr}} + (ia \mid \varpi \mid bj), \end{aligned} \tag{2}$$

where i, j are indices for occupied Kohn-Sham molecular orbitals (ψ_i, ψ_j), and a, b denotes the unoccupied Kohn-Sham orbitals (ψ_a, ψ_b), which are obtained from the ground-state DFT calculation. ϵ_i and ϵ_a are the energies of occupied and virtual orbitals, respectively. The rest of the terms in Eq. 2 considers two-electron Coulomb interactions, short-range HF exchange, long-range HF exchange, and exchange-correlation term (f_{xc}) of the employed density functional. The integrals in Eq. 2 are given by

$$\begin{aligned} (ia \mid jb) &= \int\int \psi_i(\mathbf{r}_1)\psi_a(\mathbf{r}_1)\frac{1}{r_{12}}\psi_j(\mathbf{r}_2)d\mathbf{r}_1 d\mathbf{r}_2 \\ (ij \mid ab)_{\mathrm{sr}} &= \int\int \psi_i(\mathbf{r}_1)\psi_j(\mathbf{r}_1)\frac{\mathrm{erfc}(\omega r_{12})}{r_{12}}\psi_a(\mathbf{r}_2)\psi_b(\mathbf{r}_2)d\mathbf{r}_1 d\mathbf{r}_2 \\ (ij \mid ab)_{\mathrm{lr}} &= \int\int \psi_i(\mathbf{r}_1)\psi_j(\mathbf{r}_1)\frac{\mathrm{erf}(\omega r_{12})}{r_{12}}\psi_a(\mathbf{r}_2)\psi_b(\mathbf{r}_2)d\mathbf{r}_1 d\mathbf{r}_2 \\ (ia \mid \varpi \mid jb) &= \int \psi_i(\mathbf{r})\psi_a(\mathbf{r})\frac{\partial^2 f_{\mathrm{xc}}}{\partial \rho^2}\psi_j(\mathbf{r})\psi_b(\mathbf{r})d\mathbf{r}, \end{aligned} \tag{3}$$

where erf(ωr_{12}) and erfc(ωr_{12}) are the error function and complementary error function, respectively. At the Tamm-Dancoff approximation (TDA), the B matrix is set to zero yielding

$$AX = \Delta EX\,. \tag{4}$$

At the HF level, *i.e.*, with 100% short-range and long-range HF exchange and 0% exchange-correlation contribution, Eq. 1 is the HF linear response equation also known as the random-phase approximation (RPA).[83,84] Eq. 4 corresponds to the configuration interaction singles (CIS) level.[85,86] The TDA (CIS) and TDDFT (RPA) equations are usually solved using direct diagonalization methods.[47,48,87]

2.2 Considered DFT functionals

In the present study, vertical excitation energies (VEE) have been calculated at the following levels:

- CIS and RPA levels using HF orbitals and orbital energies.
- TDDFT level using the BP86[77–79] and PBE[88,89] GGA functionals without HF exchange as well as the M11-L[90] range-separated meta-GGA functional that does not contain any HF exchange term.
- TDDFT level using the B3LYP[72–74] and PBE0[91] hybrid functionals with 20% and 25% HF exchange, respectively.
- TDDFT level using the BHLYP[92] functional with 50% HF exchange and the PBE50 functional with 50% PBE exchange, 50% HF exchange and 100%PBE correlation as well as the M06-2X functional, which is a meta-GGA hybrid functional with 54% HF exchange.[93]
- TDDFT level using range-separated functionals. The amount of short-range and long-range HF exchange is given in Table 1. The employed range-separated functionals are: CAM-B3LYP,[70] ωPBE,[82,94] ωPBEh,[82] ωB97X,[81] ωB97X-D,[71] BNL[95,96] and M11.[97]
- TDDFT level using our empirical parameterization of the CAM-B3LYP and ωPBE0 functionals with 50% long-range HF exchange. The amount of HF exchange in our CAMh-B3LYP and ωhPBE0 functionals are given in Table 1.

The exact shape of the long-range exchange-correlation potential corresponds to 100% Hartree-Fock exchange. However, functionals whose exchange-correlation potential corresponds to a smaller amount of Hartree-Fock exchange, such as CAM-B3LYP (65%) or here CAMh-B3LYP (50%) may suffer from charge transfer problems. However, studies have shown that around 50% Hartree-Fock exchange in the functional is in general enough to avoid spurious charge-transfer states to enter among the lowest excited states.[31,37,38,63,65,82,98,99]

2.3 Benchmark Set

The investigated molecules comprise analogs of the biochromophores from the photoactive yellow protein (PYP), the green fluorescent protein (GFP), rhodopsin/bacteriorhodopsin (Rh/bR), which have been thoroughly studied in previous works.[54,57] The molecular structures are shown in Figure 1 and the Cartesian coordinates are given as supporting information (SI). The investigated molecules are:

- PYP chromophore models: *p*-vinyl phenol (pVP), *trans-p*-coumaric acid (pCA), deprotonated *trans-p*-coumaric acid (pCA$'^{-}$), *trans-p*-coumarate (pCA$''^{-}$), thiomethyl-*p*-coumarate (TMpCA^{-}), and thiophenyl *p*-coumarate (pCT^{-}). The doubly ionic (pCA^{2-}) chromophore of the benchmarking set by Send *et al.*[57] was not included in our current data set, because doubly charge anions not generally bound without counter anions.
- GFP chromophore models: the anionic, neutral, and cationic models of *p*-hydroxy-benzyledene imidazolinone models pHBDI^{-}, pHBDI, pHBDI^{+}.
- Rh/bR chromophore models: the protonated Schiff base retinal model PSBT^{+} (all-*trans*) with a butyl group that mimics the lysine residue of the retinal protein, and PSB11Me$_2^{+}$ (11-*cis* retinal), with two methyl groups connected to the Schiff base nitrogen.

The molecular structures were optimized at the B3LYP/def2-SVP level[72–74,100] using TURBOMOLE v6.3.[101,102] The same molecular structures were used at all employed levels of theory, which is may introduce some uncertainties in the calculated VEEs.[31] However, optimizing the molecular structures at each theory level would also introduces uncertainties, as all functionals do not yield accurate molecular structures.

The VEEs calculated using the B3LYP structures differ by less than 0.05 eV from those obtained at the same level of theory using the molecular structures optimized at the second-order Møller-Plesset level.[57] (See Table S1 in the SI). Excitation energies were calculated using the Q-Chem v4.1[103,104] using the DFT functionals presented in Section 2.2. The def2-TZVP[105] and aug-def2-TZVP[106] Karlsruhe basis sets were used, where aug denotes that the basis sets were augmented with diffuse functions from Dunning's aug-cc-pVTZ basis set.[107] The root mean square (RMS) deviation and the mean signed average (MSA) deviation relative to the excitation energies calculated at the CC2 level were obtained as

$$\mathrm{RMS} = \sqrt{\frac{\sum_{i=1}^{N}(\mathrm{VEE}_{\mathrm{TDDFT},i} - \mathrm{VEE}_{\mathrm{CC2},i})^2}{N}}$$
$$\mathrm{MSA} = \frac{\sum_{i=1}^{N}(\mathrm{VEE}_{\mathrm{TDDFT},i} - \mathrm{VEE}_{\mathrm{CC2},i})}{N}. \quad (5)$$

2.4 Protein models

The performance of the functionals on large protein models were investigated by calculating VEEs at the B3LYP, CAM-B3LYP, CAMh-B3LYP level using the def2-TZVP basis sets.[105] The obtained results are compared to experimental data and to VEEs calculated at the CC2

level on DFT-optimized protein models of the green fluorescent protein (GFP) and the retinoid-binding protein II (hCRBPII) shown in Figure 2.

The hCRBPII models were constructed as described in Ref. 109. They are based on the X-ray structures whose PDB IDs are 4EXZ (model S2), 4EFG (model S3), and 4EEJ (model S6).[110] The protein models comprise the retinal chromophore, and the first/second sphere of amino acid residues, as well as Lys-108, which is covalently linked to the retinyl moiety by a protonated Schiff base. To simulate the rigidity of the protein backbone, the amino acids were cut at the C_β-positions and saturated with hydrogen atoms. The protein models consist of 170-190 atoms. All proteins models were optimized at the B3LYP-D3/def2-SVP level using COSMO with relative dielectric constant (ϵ) of 4.[72–74,100,111,112] The references VEE values were calculated at the CC2/def2-TZVP level with virtual orbitals higher than 70 eV above the highest occupied molecular orbital (HOMO) frozen.

The protein models for GFP were constructed based on the X-ray structure of the protein from Aequorea victoria (PDB ID:1EMB), as described in Refs 10 and 11. The protein models comprise the pHBDI chromophore, and first sphere amino acid residues and five surrounding water molecules. The protein residues were cut at the C_β-positions, which were saturated with hydrogen atoms and fixed during structure optimization at the B3LYP/def2-SVP/ϵ = 4 level. The GFP models, comprising 161 atoms, were optimized in the A and B forms of the GFP photocycle, with the phenol group of pHBDI protonated/Glu-222 deprotonated and pHBDI deprotonated/Glu-222 protonated, respectively. The VEE references values were calculated at the CC2/def2-TZVP level with virtual orbitals higher than 60 eV above the HOMO frozen.

3 Results and discussion

3.1 Analysis of the five lowest excitations

The five lowest VEEs of the 11 biochromophore analogs were computed at the CIS, RPA, TDA and TDDFT levels using def2-TZVP and aug-def2-TZVP basis sets. The TDA and TDDFT excitation energies calculated using the def2-TZVP and aug-def2-TZVP basis sets are plotted against the corresponding CC2 values in Figures 3 and 4, respectively. The lowest VEEs obtained at each level are summarized in Table S1. All calculated VEEs and oscillator strengths are compared in Tables S2–S12 with reference CC2 values calculated by Send *et al.*[57] Figures 3 and 4 show that calculations with 100% HF exchange, *i.e.*, CIS/RPA severely overestimates the excitation energies, while pure functionals (BP86, PBE, and M11-L) with 0% HF exchange, tend to underestimate the excitation energies, which is consistent with several previous studies (See Ref. 37). One can also see in the figures that functionals with intermediate amount of short-range and long-range HF exchange yield excitation energies in better agreement with the CC2 values. The RMS and MSA deviations of the excitation energies relatively to the CC2 values are shown in Figure 5, whose raw data are given in Tables S13 and S14.

Note that both the oscillator strengths and the orbital character have to be considered in order to confirm that the VEEs of the same states are compared. It is a very comprehensive task that would most like to lead to a general improvment of the performance of the hybrid

functionals, because charge transfer effects and spurious dark low-lying states are more common for pure density functionals.

3.1.1 B3LYP, BHLYP, CAM-B3LYP and CAMh-B3LYP—The amount of HF exchange in the three hybrid functionals B3LYP (20%), BHLYP (50%), and CAM-B3LYP (19% short-range, 65% long-range) strongly affects the calculated excitation energies as shown in Figures 3 and 4, as well as in Figure 5, whose raw data are given in Tables S13 and S14. The B3LYP functional with a def2-TZVP (aug-def2-TZVP) basis underestimates the VEEs by a MSA of −0.39 eV (−0.31 eV) relative to CC2, whereas BHLYP overestimates the respective VEEs by 0.34 eV (0.35 eV). For the CAM-B3LYP functional we obtain a MSA of 0.18 eV (0.25 eV). The CAM-B3LYP functional performs on average somewhat better than the B3LYP and BHLYP functionals.

The sign of the MSA deviations indicates that the increased long-range HF exchange of the CAM-B3LYP functional overcorrects the underestimated VEEs obtained at the B3LYP level relative to the CC2 reference values. The B3LYP and CAM-B3LYP functionals contain nearly the same amount of short-range HF exchange (20% versus 19%, Table 1), suggesting that the 65% long-range HF exchange is responsible for the systematic blueshift of the VEEs in the CAM-B3LYP calculations.

Mixing the B3LYP and CAM-B3LYP functionals with a ratio of 1:2 roughly cancels the MSA values suggesting a new empirical functional with 19% short-range HF exchange and 50% long-range HF exchange, which we denote as CAMh-B3LYP, where h indicates the 50% HF exchange in the long-range part. CAMh-B3LYP calculations reproduce the CC2 results rather well as seen in Figures 3 and 4. The MSA values are 0.01 eV and 0.07 eV for the def2-TZVP and aug-def2-TZVP basis sets, respectively. The calculations also show that the CAMh-B3LYP functional not only reduces the systematic errors of the B3LYP and CAM-B3LYP, but it also improves the RMS deviations of the benchmarking set, which are 0.51 eV (B3LYP) > 0.28 eV (CAM-B3LYP) > 0.21 eV (CAMh-B3LYP) with the def2-TZVP basis sets and 0.37 eV (B3LYP) > 0.31 eV (CAM-B3LYP) > 0.16 eV (CAMh-B3LYP) with the aug-def2-TZVP basis sets. The MSA and RSM values are compared in Figure 5.

3.1.2 PBE, PBE0, PBE50, *ω*PBE, *ω*PBEh, and *ω*hPBE0—The VEEs obtained using the PBE-type functionals are shown in Figures 3 and 4, whose raw data are given in Tables S2–S12. The PBE functional using the def2-TZVP (aug–def2-TZVP) basis sets significantly underestimates the VEEs with an MSA value of −1.03 eV (−0.85 eV), while the PBE50 functional with 50% exchange overestimates the VEEs by 0.36 eV (0.43 eV, Figure 5).

The hybrid functional PBE0 (25% short-range, 25% long-range) and the range-separated *ω*PBE (100% long-range) and *ω*PBEh (20% short-range, 100 % long-range) functionals yield excitation energies in better agreement with the CC2 reference data. The obtained MSA values are −0.25 eV (−0.14 eV), 0.25 eV (0.40 eV), and 0.19 eV (0.30 eV) for PBE0, *ω*PBE, and *ω*PBEh, respectively.

By using the same mixing procedure as for the CAMh-B3LYP functional, we propose a functional with more long-range HF exchange relative to PBE0 (25%), but less than for ωPBEh (100%). The empirical ωhPBE0 functional has 25% short-range HF exchange and 50% long-range HF exchange. The obtained RMS values for the PBE-type functionals are 1.17 eV (PBE) > 0.43 eV (PBE50) > 0.38 eV (PBE0) > 0.33 eV (ωPBE) > 0.29 eV (ωPBEh) > 0.21 eV (ωhPBE0) with the def2-TZVP basis sets, and 0.95 eV (PBE) > 0.48 eV (PBE50, ωPBE) > 0.37 eV (ωPBEh) > 0.23 eV (PBE0) > 0.17 eV (ωhPBE0) with the aug-def2-TZVP basis sets (Figure 5). By further augmenting the basis set with diffuse functions could improve the performance of the PBE0 functional. However, it could also introduce charge-transfer problems, because PBE0 has only 25% HF exchange.

3.1.3 ωB97X and ωB97X-D—Although, the ωB97X-D functional was initially designed for studies of electronic ground states,[71] it was suggested that it could also be used in studies of electronic excited states.[64] The calculations yielded even better excitation energies that those obtained with the ωB97X functional.[81] Both functionals have a tendency to overestimate the VEEs of the biochromophores relative to the CC2 values as seen in Figures 3 and 4. The ωB97X-D functional has MSA values of 0.23 eV (0.36 eV) with the def2-TZVP (aug-def2-TZVP), which about half the MSA values of 0.42 eV (0.60 eV) obtained with the ωB97X functional. The RMS deviations follow the same trend with 0.31 eV (0.43 eV) and 0.50 eV (0.68 eV) at the ωB97X-D and ωB97X levels, respectively (Figure 5).

3.1.4 M06-2X, M11, and M11-L—The M06-2X, M11, and M11-L functionals are meta-GGAs that also depend on the kinetic energy density. Wheeler and Houk[113] reported that very fine numerical integration grids might be required when studying chemical reactions using meta-GGA functionals. We therefore employed two atomic grids in the numerical integration.[114] The SG-1 grid,[115] which is a pruned (50, 194) grid and an unpruned (99, 590) grid were used. We did not find any significant grid dependence, since the obtained excitation energies differ by less than 0.014 eV when using these grids.

The M06-2X functionals perform well, which is also consistent with the findings of Isegawa *et al.*[64] (Figures 3 and 4). The obtained MSA values for the M06-2X functional are 0.17-0.18 eV and the RMS values are 0.26-0.27 eV for the two basis sets. M11 also performs well with the aug-def2-TZVP basis sets (MSA=0.16, RMS=0.36 eV), whereas it has a larger error with def2-TZVP basis sets (MSA=0.36, RMS=0.44 eV). The excitation energies calculated with the M11-L functional are underestimated. The MSA values are −0.73 eV and −1.19 eV when using the def2-TZVP and aug-def2-TZVP basis sets, respectively, which agrees with the MSA values obtained with the other GGA functionals. The MSA and RMS values are shown in Figure 5.

3.1.5 Other functionals—BP86 is an old GGA functional that also underestimates the VEEs. The MSA and RMS values are −1.01 eV (−0.80 eV) and 1.14 eV (0.91 eV) with the def2-TZVP (aug-def2-TZVP) basis sets, respectively. BNL is a range-separated functional whose ω parameter one should adjust for each molecule.[116] However, here we have used the generic value of ω=0.5 for all molecules. The VEEs obtained with the BNL functional deviate significantly from the CC2 reference values. The obtained MSA and RMS values are

0.59 eV (0.63 eV) and 0.68 eV (0.70 eV), respectively, when using the def2-TZVP (aug-def2-TZVP) basis sets. The VEEs are compared with the CC2 data in Figures 3 and 4. The MSA and RMS values are given in Figure 5.

3.1.6 TDDFT *vs.* TDA—The computational costs for TDA calculations of the VEEs are somewhat smaller than for TDDFT calculations, because the size of the TDA matrices is a factor of two smaller. It is also of interest to investigate the performance of the TDA method, since a number of TDA studies has recently been reported.[117–120] The VEEs calculated at the TDA and TDDFT levels are compared with the CC2 reference values in Figures 3 and 4, whose raw data are listed in Tables S2–S12 and S15–S25. The corresponding MSA and RSM values are compared in Figure 5. The VEEs calculated at the TDDFT and TDA levels deviate in a similar manner from the CC2 values. However, the VEEs calculated using the TDA method are in general less accurate than the ones obtained in TDDFT calculations. The VEEs calculated using TDA and TDDFT methods are compared in Figures S1 and S2.

The TDDFT calculations often yield smaller excitation energies than obtained with the TDA method implying that for functional that underestimate the VEEs, the MSA values of the TDA calculations are smaller due to cancellation of errors. Larger VEEs are generally obtained with the TDA method when using GGA functionals and many hybrid functionals such as B3LYP and PBE0. However, no significant changes in the RMS values between the TDA and TDDFT calculations are obtained at the B3LYP and PBE0 levels (Figure 5). For cases where the TDA and the TDDFT calculations overestimate the VEEs, such as with the range-corrected CAM-B3LYP, CAMh-B3LYP, ωhPBE0, ωPBEh, ωB97X-D, M06-2X and M11 functionals, the TDDFT calculations yield VEEs in closer agreement with the CC2 results than with TDA. The TDA excitation energies are for some molecules more accurate than the VEEs calculated at the corresponding TDDFT level, which is most likely due to error cancellations, because TDA is an approximation to TDDFT.

3.1.7 Similarities among different functionals—Cross RMS values, shown in Figure 6 can be used to detect similarities in performance of the studied functionals. The following similarities were identified:

- The GGA functionals BP86 and PBE have generally too small VEEs and a similar cross-RMS of 0.07 eV, suggesting that VEEs are underestimated similarly by both methods.
- The two new empirically parameterized functionals CAMh-B3LYP and ωhPBE0 have a cross-RMS of 0.08 eV. Similar cross-RMS values are also obtained for the ωB97X-D, ωPBE and ωB97X-D, ωPBEh pair of functionals with 100% long-range HF exchange.
- The long-range corrected functional CAM-B3LYP has a cross-RMS of 0.10 eV with ωPBEh and 0.13 eV with M06-2X.
- BHLYP and PBE50 with 50% HF exchange have a cross-RMS of 0.13 eV.

3.2 Analysis of the lowest excited state and relative VEEs

3.2.1 Lowest excited state—The lowest excited state is often the most photobiologically relevant state for biomolecules. From a computational perspective, the lowest excited state is less prone to charge-transfer problems and does usually not have a significant Rydberg character, implying that range-separated functionals are not generally needed when studying them.

The RMS of the B3LYP functional diminishes from 0.37 eV to 0.26 eV, when considering only the lowest excited state instead of the five lowest states using the aug-def2-TZVP basis sets. For the range-separated CAM-B3LYP functional, the RMS values obtained for the lowest state and for the five lowest states are 0.31 eV and 0.26 eV, respectively. The RMS values for the two new functionals (CAMh-B3LYP and ωhPBE0) are almost the same for the first excited state (0.16-0.17 eV) and the five lowest excited states (0.18-0.19 eV), respectively. In contrast to the CAM-B3LYP functionals and the ωhPBE0 functional, the RMS value of the first state is significantly better than for the five lowest states for the other range-separated functionals: ωPBE (0.48 eV → 0.23 eV), ωPBEh (0.37 eV → 0.24 eV), ωB97X-D (0.68 → 0.26 eV). The M11 functional has a better RMS value of 0.25 eV for the first excited state as compared to 0.36 eV for the five lowest states, while the RMS values for the M06-2X and M11-L are almost the same for the first and the five first excited states. Similar trends are obtained with the def2-TZVP level basis set. All RMS values are reported in Tables S13 and S14 and summarized in Figures S3 and S4.

A complication that appears when comparing VEEs calculated using different functionals is that the photochemically relevant bright state may not always be the lowest excited state.[57] Thus, oscillator strengths and orbital character have to be considered in order to assess whether the VEEs of the same states are compared. Such an analysis is more comprehensive and outside the scope of this work. However, it would most like to lead to a general improved performance of the hybrid functionals, because charge transfer effects and spurious dark low-lying states are more common for pure density functionals.

3.2.2 Relative excitation energies—In calculations of surface crossings or spectral overlap in fluorescence resonance energy transfer (FRET), the optical gaps between different excited states is more important than the absolute VEEs. The deviations of the TDDFT and TDA excitation energies with respect to the CC2 values are shown in Tables S2–S12 and Tables S15–S25 and summarized in Figure 5. For many of the functionals, the RMS values for the relative VEEs are much smaller than for vertical transition energy from the ground state. The RMS values obtained using the aug-def2-TZVP basis sets are CAM-B3LYP (0.12 eV), M06-2X (0.13 eV), CAMh-B3LYP (0.15 eV), BHLYP (0.17 eV), ωhPBE0 (0.19 eV), and ωPBEh (0.20 eV), all of which reproduce best the CC2 results for the current data set.

3.3 Mixed basis sets

For the 11 molecules studied here, the number of basis functions is 327-1003 with the def2-TZVP basis sets and 573-1745 with the aug-def2-TZVP basis sets. Adding diffuse functions to the def2-TZVP basis sets improves the accuracy of the VEEs of states with performance for with significant Rydberg character. However, the computational costs are 3-5 times

higher. In order to avoid the significant increase in computational efforts, we employed a mixed basis set, where the diffuse functions are placed only on the hydrogen atoms, which lie mainly at the outer edge of the chromophore. Diffuse molecular centered basis functions has also been used for reducing the computational costs when studying excited states with significant Rydberg character.[121] The use of the mixed basis set leads to a small increase of about 25% in the computational time as compared to the calculations with the def2-TZVP basis sets.

We studied eight of the molecules with the mixed basis sets, listed in Figure 1. We omitted pHBDI$^+$, PSBT$^+$, PSB11Me$_2^+$, which are cations with a very small basis-set dependence of the calculated VEEs. The largest difference between the VEEs obtained with the def2-TZVP and aug-def2-TZVP basis sets is 0.07 eV. We calculated VEEs using eight functionals and the mixed basis sets. The obtained results for each of the molecules are reported in Tables S26–S33 and summarized in Table S34.

For def2-TZVP basis sets, the VEEs deviate from aug-def2-TZVP values with MSA values of 0.32-0.51 eV and RMS values of 0.47-0.69 eV. With the mixed basis sets, the MSA and RMS values relatively to the aug-def2-TZVP data are only 0.05-0.09 eV and 0.09-0.13 eV, respectively.

The mixed basis sets better reproduce not only the VEEs, but also the character of the wave functions of the excited states, which was assessed by calculating the overlap attachment S_{12}^A and detachment S_{12}^D integrals for the five excited states, defined as

$$S_{12}^A = \int (\rho_1^A(\mathbf{r}))^{\frac{1}{2}} (\rho_2^A(\mathbf{r}))^{\frac{1}{2}} d\mathbf{r},$$
$$S_{12}^D = \int (\rho_1^D(\mathbf{r}))^{\frac{1}{2}} (\rho_2^D(\mathbf{r}))^{\frac{1}{2}} d\mathbf{r} \quad (6)$$

where ρ_1^A and ρ_2^A are attachment densities with basis sets 1 and 2, and ρ_1^D and ρ_2^D are the corresponding detachment densities.[122] For identical basis sets 1 and 2, the overlap integrals are equal to 1, reflecting that one electron is excited from the occupied space into the virtual space.

The overlap integrals computed from TDA calculations for the pVP molecule are given in Table S35 for the B3LYP and CAM-B3LYP functionals. At the B3LYP level using the def2-TZVP and aug-def2-TZVP basis sets, the wave functions of the five lowest excited states have S_{12}^D values of 0.99, 0.97, 0.97, 0.82, and 0.94, indicating that all states except the fourth one have nearly identical detachment densities. The corresponding overlap integrals of attachment densities (S_{12}^A) are 0.99, 0.24, 0.24, 0.37, and 0.28, suggesting that the second to fifth excited states have significant Rydberg characters. The mixed basis-set calculations yield attachment and detachment densities that are very similar to the ones obtained with the aug-def2-TZVP basis sets, since the S_{12}^A and S_{12}^D overlaps are all larger than 0.98. The same behavior was obtained at the CAM-B3LYP level as shown in Table S35.

3.4 Comparison to experimental values

CC2 calculations generally reproduce experimental excitation energies within 0.2 eV, if the ground state of the molecule does not have a significant multireference character or the double excitations from the ground state are needed for an accurate description of the excited state.[38,123–126]

Direct comparison of calculated VEEs to the experimental spectrum is difficult as the peaks of the spectrum are broadened by *e.g.*, vibrational and dynamical effects as well as due to intensity borrowing for weak transitions. We follow here the common convention to compare calculation VEEs with the experimental peak maximum.[127–129] The lowest VEEs are compared with the experimental absorption maxima in Table S36. However, some of the experimental values have been measured in solvents, in the protein or extrapolated towards to the expected vacuum absorption maxima (pHBDI chromophores) rendering it difficult to accurately determine the deviations of the calculated VEEs from experimental values. Nevertheless, when neglecting this source of uncertainty, 11 of 15 VEEs calculated at the CC2 level agree within 0.25 eV from the experimental values. The VEEs deviating less than 0. 25 eV from the experimental values are marked in bold font in Table S36. The functionals that best reproduce the available experimental data are: B3LYP (12 out of 15 values within 0.25 eV deviation), PBE0 (7 out of 15 values), and ωhPBE0 (6 out of 15 values). However, B3LYP and PBE0 tend to underestimate the VEEs for higher excited states that might have significant Rydberg state characters. Interestingly, all TDDFT functionals predict blueshifted VEEs for the first excited state of the retinal models.

3.5 Performance on protein models

The VEEs computed at the B3LYP, CAM-B3LYP, and CAMh-B3LYP levels for the protein models described in Section 2.4 and shown in Figure 2 are reported in Table 2, where the obtained energies are compared to VEEs calculated at the CC2 level and to experimental data. The VEEs calculated at the CC2 level agree within 0.1 eV with the absorption maximum in the experimental spectra. For the A and B forms of the GFP models, the B3LYP functional yields almost the same VEEs, whereas the CAM-B3LYP functional overestimates the VEE of the A form. The proposed CAMh-B3LYP functional yields VEEs in good agreement with CC2 values and with experimental data.

Calculations of VEEs of retinal proteins are also challenging at the TDDFT level using commonly used functionals, because the photoexcitation leads to a transfer of positive charge from the protonated Schiff base to the β-ionine unit. The B3LYP functional severely underestimates the VEEs by about 0.7 eV, whereas CAM-B3LYP overestimates them with a mean error of 0.27 eV. The proposed CAMh-B3LYP functional also overestimates the VEEs with a slightly improved mean error of 0.22 eV. The TDDFT calculations suggest that not only charge transfer but also correlation effects are important for accurate modelling of excited states of retinal proteins. Multiconfiguration effects are not significant, because the mean error of the VEEs calculated at the CC2 level is less than 0.05 eV. The calculations on the protein models suggest that the new CAMh-B3LYP functional may be useful for studies of excited states of large photobiological protein models.

4 Conclusions

We have computationally studied the excitation energies of the five lowest excited singlet states of 11 chemical analogs of PYP, GFP, and Rh/bR chromophores at the CIS, RPA, TDA and TDDFT levels using the def2-TZVP and aug-def2-TZVP basis sets. In the TDA and TDDFT calculations, 17 density functionals were employed including 7 existing range-separated functionals and two new empirical range-separated functionals that have 50% long-range HF exchange. The VEEs are compared with previously reported benchmark data calculated at the CC2 level. The main conclusions are:

1. Pure density functionals (BP86, PBE, M11-L) and hybrid functionals with 20% or 25% of HF exchange (B3LYP, PBE0) have a tendency of consistently underestimating VEEs. Hybrid density functionals with 50% or 54% HF exchange (BHLYP, PBE50 and M06-2X) and long-range corrected functionals (CAM-B3LYP, ωPBE, ωPBEh, ωB97XD, and M11) yield results in closer agreement with CC2 values. However, they overestimate the VEEs of excitation the present benchmarking set. The two new empirical functionals (CAMh-B3LYP and ωhPBE0) have smaller deviations from the CC2 data than the other employed functionals.
2. For the five lowest VEEs, the best performance is obtained with the CAMh-B3LYP (RMS=0.16, MSA=0.07 eV); ωhPBE0 (RMS=0.17, MSA = 0.06 eV); PBE0 (RMS=0.23, MSA=−0.14 eV); M06-2X (RMS=0.26, MSA=0.17 eV); CAM-B3LYP (RMS=0.31, MSA=0.25 eV); M11 (RMS=0.36, MSA = 0.16 eV) and ωPBEh (RMS=0.37, MSA=0.30 eV) when using the aug-def2-TZVP basis sets.
3. TDA calculations can yield smaller MSA errors that TDDFT calculations due to cancellation of errors, when using density functionals that underestimate the VEEs, while for range-separated functionals (CAM-B3LYP, CAMh-B3LYP, ωhPBE0, ωPBEh, ωB97X-D) and for functionals with more HF exchange (M06-2X and M11), the VEEs calculated at the TDDFT level are in better agreement with CC2 data.
4. For the lowest excited singlet state (S_1), the B3LYP, PBE0 and M06-2X functionals yield similar results as obtained with the range-separated functionals (CAM-B3LYP, CAMh-B3LYP, ωPBE, ωhPBE0, ωPBEh, ωB97X-D) when using the aug-def2-TZVP basis sets.
5. The most accurate transition energies between excited states for the current photobiological data set are obtained with the M06-2X, CAM-B3LYP, CAMh-B3LYP, BHLYP, ωhPBE0, and ωPBEh functionals.
6. When using aug-def2-TZVP basis functions on only the hydrogen atoms, the computational costs increase by about 25% as compared to calculations using the def2-TZVP basis sets, while the MSA deviates by less than 0.1 eV from the values obtained with the aug-def2-TZVP basis sets.

7. The proposed CAMh-B3LYP functional improves the accuracy of calculated VEEs for large protein models.

Supplementary Material

Refer to Web version on PubMed Central for supplementary material.

Acknowledgments

The Biowulf cluster at NIH is acknowledged for computer time. We thank Dr. Bernard Brooks for providing additional computational resources on the LoBoS computer system at NIH. The authors acknowledge Prof. Andreas Dreuw for insightful discussion. The work was supported in part by the U.S. Depart of Energy under Grant No. DE-SC0011297, and the Jane and Aatos Erkko foundation. This research was also supported by the Academy of Finland (314821), Magnus Ehrnrooth Foundation, and the Swedish Cultural Foundation in Finland.

References

(1). Coto PB; Strambi A; Ferre N; Olivucci M The color of rhodopsins at the ab initio multiconfigurational perturbation theory resolution. Proc. Natl. Acad. Sci. USA 2006, 103, 17154–17159. [PubMed: 17090682]

(2). Zhou X; Sundholm D; Wesolowski TA; Kaila VRI Spectral Tuning of Rhodopsin and Visual Cone Pigments. J. Am. Chem. Soc 2014, 136, 2723–2726. [PubMed: 24422511]

(3). Fujimoto K; Hayashi S; Hasegawa H-Y; Nakatsuji H Theoretical studies on the color-tuning mechanism in retinal proteins. J. Chem. Theory Comput. 2007, 3, 605–618. [PubMed: 26637039]

(4). Bravaya KB; Khrenova MG; Grigorenko BL; Nemukhin AV; Krylov AI Effect of Protein Environment on Electronically Excited and Ionized States of the Green Fluorescent Protein Chromophore. J. Chem. Phys. B 2011, 115, 8296–8303.

(5). Castro A; Marques MA; Varsano D; Sottile F; Rubio A The challenge of predicting optical properties of biomolecules: What can we learn from time-dependent density-functional theory? Comptes Rendus Phys. 2009, 10, 469–490.

(6). Neugebauer J Subsystem-Based Theoretical Spectroscopy of Biomolecules and Biomolecular Assemblies . Chem. Phys. Chem 2009, 10, 3148–3173. [PubMed: 19911405]

(7). Wanko M; Garca-Risueo P; Rubio A Excited states of the green fluorescent protein chromophore: Performance of ab initio and semi-empirical methods. Phys. Stat. Solidi (b) 2012, 249, 392–400.

(8). Altun A; Yokoyama S; Morokuma K Mechanism of Spectral Tuning Going from Retinal in Vacuo to Bovine Rhodopsin and its Mutants: Multireference ab Initio Quantum Mechanics/Molecular Mechanics Studies. J. Chem. Phys. B 2008, 112, 16883–16890.

(9). Valsson O; Campomanes P; Tavernelli I; Rothlisberger U; Filippi C Rhodopsin Absorption from First Principles: Bypassing Common Pitfalls. J. Chem. Theory Comput. 2013, 9, 2441–2454. [PubMed: 26583734]

(10). Send R; Suomivuori C-M; Kaila VRI; Sundholm D Coupled-Cluster Studies of Extensive Green Fluorescent Protein Models Using the Reduced Virtual Space Approach. J. Phys. Chem. B 2015, 119, 2933–2945. [PubMed: 25613980]

(11). Kaila VRI; Send R; Sundholm D Electrostatic spectral tuning mechanism of the green fluorescent protein. Phys. Chem. Chem. Phys 2013, 15, 4491–4495. [PubMed: 23420178]

(12). Adamo C; Jacquemin D The calculations of excited-state properties with Time-Dependent Density Functional Theory. Chem. Soc. Rev 2013, 42, 845–856. [PubMed: 23117144]

(13). Santoro F; Barone V; Improta R Can TD-DFT calculations accurately describe the excited states behavior of stacked nucleobases? The cytosine dimer as a test case. J. Comp. Chem 2008, 29, 957–964. [PubMed: 17963224]

(14). Suomivuori C-M; Winter NOC; Hattig C; Sundholm D; Kaila VRI Exploring the Light-Capturing Properties of Photosynthetic Chlorophyll Clusters Using Large-Scale Correlated Calculations. J. Chem. Theory Comput. 2016, 12, 2644–2651. [PubMed: 27153186]

(15). Kaila VRI; Send R; Sundholm D The effect of the protein environment on primary photo-excitation events of retinal: Photorhodopsin and thermal isomerization. J. Phys. Chem. B 2012, 116, 2249–2258. [PubMed: 22166007]

(16). Harbach PHP; Wormit M; Dreuw A The third-order algebraic diagrammatic construction method (ADC(3)) for the polarization propagator for closed-shell molecules: Efficient implementation and benchmarking. J. Chem. Phys 2014, 141, 064113. [PubMed: 25134557]

(17). Mancini DT; Sen K; Barbatti M; Thiel W; Ramalho TC Excited-State Proton Transfer Can Tune the Color of Protein Fluorescent Markers. ChemPhysChem 2015, 16, 3444–3449. [PubMed: 26333875]

(18). Gao X; Bai S; Fazzi D; Niehaus T; Barbatti M; Thiel W Evaluation of Spin-Orbit Couplings with Linear-Response Time-Dependent Density Functional Methods. J. Chem. Theory Comput. 2017, 13, 515–524. [PubMed: 27959528]

(19). Lischka H; Nachtigalkwa D; Aquino AJA; Szalay PG; Plasser F; Machado FBC; Barbatti M Multireference Approaches for Excited States of Molecules. Chem. Rev 2018, 118, 7293–7361. [PubMed: 30040389]

(20). Jacquemin D What is the Key for Accurate Absorption and Emission Calculations, Energy or Geometry? J. Chem. Theory Comput. 2018, 14, 1534–1543. [PubMed: 29365256]

(21). Jornet-Somoza J; Alberdi-Rodriguez J; Milne BF; Andrade X; Marques MAL; Nogueira F; Oliveira MJT; Stewart JJP; Rubio A Insights into colour-tuning of chlorophyll optical response in green plants. Phys. Chem. Chem. Phys 2015, 17, 26599–26606. [PubMed: 26250099]

(22). Suomivuori CM; Gamiz-Hernandez AP; Sundholm D; Kaila VRI Energetics and dynamics of a light-driven sodium-pumping rhodopsin. Proc. Natl. Acad. Sci. USA 2017, 114, 7043–7048. [PubMed: 28611220]

(23). Gamiz-Hernandez AP; Neycheva IA; Send R; Sundholm D; Kaila VRI Protein-Induced Color Shift of Carotenoids in β-Crustacyanin. Angew. Chem. Int. Ed 2015, 54, 11564–11566.

(24). Gamiz-Hernandez AP; Kaila VRI Conversion of Light-Energy Into Molecular Strain in the Photocycle of the Photoactive Yellow Protein. Phys. Chem. Chem. Phys 2016, 18, 2802–2809. [PubMed: 26726853]

(25). Runge E; Gross EKU Density-Functional Theory for Time-Dependent Systems. Phys. Rev. Lett 1984, 52, 997–1000.

(26). Casida ME In Recent Advances in Density Functional Methods, Vol. 1; Chong DP, Ed.; World Scientific: Singapore, 1995; pp 155–192.

(27). Furche F; Ahlrichs R Adiabatic time-dependent density functional methods for excited state properties. J. Chem. Phys 2002, 117, 7433–7447.

(28). Marques MAL; Gross EKU Time-dependent density functional theory. Ann. Rev. Phys. Chem 2004, 55, 427–455. [PubMed: 15117259]

(29). Burke K; Werschnik J; Gross EKU Time-dependent density functional theory: past, present, and future. J. Chem. Phys 2005, 123, 62206. [PubMed: 16122292]

(30). Rappoport D; Furche F In Time-Dependent Density Functional Theory; Marques MAL, Ullrich CA, Nogueira F, Rubio A, Burke K, Gross EKU, Eds.; Lecture Notes in Physics 706; Springer-Verlag, 2006; pp 337–354.

(31). Dreuw A; Head-Gordon M Single-Reference ab initio Methods for the Calculation of Excited States of Large Molecules. Chem. Rev 2005, 105, 4009–4037. [PubMed: 16277369]

(32). Casida ME; Huix-Rotllant M Progress in time-dependent density-functional theory. Ann. Rev. Phys. Chem 2012, 63, 287–323. [PubMed: 22242728]

(33). Ekstrom U; Visscher L; Bast R; Thorvaldsen AJ; Ruud K Arbitrary-Order Density Functional Response Theory from Automatic Differentiation. J. Chem. Theory Comput. 2010, 6, 1971–1980. [PubMed: 26615926]

(34). Marques MAL; Oliveira MJT; Burnus T Libxc: A library of exchange and correlation functionals for density functional theory. Comput. Phys. Commun 2012, 183, 2272–2281.

(35). Mardirossian N; Head-Gordon M Thirty years of density functional theory in computational chemistry: an overview and extensive assessment of 200 density functionals. Mol. Phys 2017, 115, 2315–2372.

(36). Lehtola S; Steigemann C; Oliveira MJ; Mar ques MA Recent developments in LIBXC – A comprehensive library of functionals for density functional theory. SoftwareX 2018, 7, 1–5.

(37). Dreuw A; Head-Gordon M Failure of Time-Dependent Density Functional Theory for Long-Range Charge-Transfer Excited States: The Zincbacteriochlorin - Bacteriochlorin and Bacteriochlorophyll - Spheroidene Complexes. J. Am. Chem. Soc 2004, 126, 4007–4016. [PubMed: 15038755]

(38). Lehtonen O; Sundholm D; Send R; Johansson MP Coupled-cluster and density functional theory studies of the electronic excitation spectra of *trans*-1,3-butadiene and *trans*-2-propeniminium. J. Chem. Phys 2009, 131, 024301. [PubMed: 19603985]

(39). Christiansen O; Koch H; Jorgensen P The second-order approximate coupled cluster singles and doubles model CC2. Chem. Phys. Lett 1995, 243, 409–418.

(40). Hattig C; Weigend F CC2 excitation energy calculations on large molecules using the resolution of the identity approximation. J. Chem. Phys 2000, 113, 5154.

(41). Send R; Kaila VRI; Sundholm D Reduction of the virtual space for coupled-cluster excitation energies of large molecules and embedded systems. J. Chem. Phys 2011, 134 , 214114. [PubMed: 21663351]

(42). Kaila R, Ville RI Send; Sundholm, D. Electrostatic spectral tuning mechanism of the green fluorescent protein. Phys. Chem. Chem. Phys 2013, 15, 4491–4495. [PubMed: 23420178]

(43). Winter NOC; Hattig C Scaled opposite-spin CC2 for ground and excited states with fourth order scaling computational costs. J. Chem. Phys 2011, 134, 184101. [PubMed: 21568491]

(44). Rhee YM; Head-Gordon M Scaled Second-Order Perturbation Corrections to Configuration Interaction Singles: Efficient and Reliable Excitation Energy Methods. J. Phys. Chem. A 2007, 111, 5314–5326. [PubMed: 17521172]

(45). Ovchinnikov VA; Sundholm D Coupled-cluster and density functional theory studies of the electronic 0-0 transitions of the DNA bases. Phys. Chem. Chem. Phys 2014, 16, 6931–6941. [PubMed: 24595333]

(46). Benkyi I; Tapavicza E; Fliegl H; Sundholm D Calculation of vibrationally resolved absorption spectra of acenes and pyrene. Phys. Chem. Chem. Phys 2019, 21, 21094–21103. [PubMed: 31528954]

(47). Hirata S; Head-Gordon M Time-dependent density functional theory for radicals: An improved description of excited states with substantial double excitation character. Chem. Phys. Lett 1999, 302, 375–382.

(48). Hirata S; Head-Gordon M Time-dependent density functional theory within the TammDancoff approximation. Chem. Phys. Lett 1999, 314, 291–299.

(49). Hsu C-P; Hirata S; Head-Gordon M Excitation Energies from Time-Dependent Density Functional Theory for Linear Polyene Oligomers: Butadiene to Decapentaene. J. Phys. Chem. A 2001, 105, 451–458.

(50). Dierksen M; Grimme S The Vibronic Structure of Electronic Absorption Spectra of Large Molecules : A Time-Dependent Density Functional Study on the Influence of Exact Hartree - Fock Exchange. J. Phys. Chem. A 2004, 108, 10225–10237.

(51). Silva-Junior MR; Schreiber M; Sauer SPA; Thiel W Benchmarks for electronically excited states: time-dependent density functional theory and density functional theory based multireference configuration interaction. J. Chem. Theory Comput. 2008, 129, 104103.

(52). Jacquemin D; Wathelet V; Perpete EA; Adamo C Extensive TD-DFT Benchmark: Singlet-Excited States of Organic Molecules. J. Chem. Theory Comput. 2009, 5, 2420–2435. [PubMed: 26616623]

(53). Stein T; Kronik L; Baer R Reliable prediction of charge transfer excitations in molecular complexes using time-dependent density functional theory. J. Am. Chem. Soc 2009, 131, 2818–2820. [PubMed: 19239266]

(54). Ma Y; Rohlfing M; Molteni C Modeling the Excited States of Biological Chro-mophores within Many-Body Green's Function Theory. J. Chem. Theory Comput 2010, 6, 257–265. [PubMed: 26614336]

(55). Caricato M; Trucks GW; Frisch MJ; Wiberg KB Electronic Transition Energies: A Study of the Performance of a Large Range of Single Reference Density Functional and Wave Function

Methods on Valence and Rydberg States Compared to Experiment. J. Chem. Theory Comput. 2010, 6, 370–383. [PubMed: 26617296]

(56). Liu F; Gan Z; Shao Y; Hsu C-P; Dreuw A; Head-Gordon M; Miller BT; Brooks BR; Yu J-G; Furlani TR et al. A parallel implementation of the analytic nuclear gradient for time-dependent density functional theory within the Tamm-Dancoff approximation. Mol. Phys 2010, 108, 2791–2800.

(57). Send R; Kaila VRI; Sundholm D Benchmarking the Approximate Second-Order Coupled-Cluster Method on Biochromophores. J. Chem. Theory Comput. 2011, 7, 2473–2484. [PubMed: 26606621]

(58). Send R; Kuhn M; Furche F Assessing Excited State Methods by Adiabatic Excitation Energies. J. Chem. Theory Comput. 2011, 7, 2376–2386. [PubMed: 26606613]

(59). Nguyen KA; Day PN; Pachter R The performance and relationship among range-separated schemes for density functional theory. J. Chem. Phys 2011, 135, 074109. [PubMed: 21861558]

(60). Mardirossian N; Parkhill JA; Head-Gordon M Benchmark results for empirical post-GGA functionals : Difficult exchange problems and independent tests. Phys. Chem. Chem. Phys 2011, 13, 19325–19337. [PubMed: 21956624]

(61). Peach MJG; Tozer DJ Overcoming Low Orbital Overlap and Triplet Instability Problems in TDDFT. J. Phys. Chem. A 2012, 116, 9783–9789. [PubMed: 22971224]

(62). Leang SS; Zahariev F; Gordon MS Benchmarking the performance of time-dependent density functional methods. J. Chem. Phys 2012, 136, 104101. [PubMed: 22423822]

(63). Dev P; Agrawal S; English NJ Determining the appropriate exchange-correlation functional for time-dependent density functional theory studies of charge-transfer excitations in organic dyes. J. Chem. Phys 2012, 136, 224301. [PubMed: 22713041]

(64). Isegawa M; Peverati R; Truhlar DG Performance of recent and high-performance approximate density functionals for time-dependent density functional theory calculations of valence and Rydberg electronic transition energies. J. Chem. Phys 2012, 137, 244104. [PubMed: 23277925]

(65). Charaf-Eddin A; Planchat A; Mennucci B; Adamo C; Jacquemin D Choosing a Functional for Computing Absorption and Fluorescence Band Shapes with TD-DFT. J. Chem. Theory Comput. 2013, 9, 2749–2760. [PubMed: 26583866]

(66). Fang C; Oruganti B; Durbeej B How Method-Dependent Are Calculated Differences between Vertical, Adiabatic, and 0-0 Excitation Energies? J. Phys. Chem. A 2014, 118, 4157–4171. [PubMed: 24848558]

(67). Laurent AD; Jacquemin D TD-DFT benchmarks: A review. Int. J. Quantum Chem. 2013, 113, 2019–2039.

(68). Zhao Y; Truhlar DG The M06 suite of density functionals for main group thermochemistry, thermochemical kinetics, noncovalent interactions, excited states, and transition elements: Two new functionals and systematic testing of four M06-class functionals and 12 other functionals. Theo. Chem. Acc 2008, 120, 215–241.

(69). Perdew JP; Burke K; Ernzerhof M Rationale for mixing exact exchange with density functional approximations. J. Chem. Phys 1996, 105, 9982–9985.

(70). Yanai T; Tew DP; Handy NC A new hybrid exchange-correlation functional using the Coulomb-attenuating method (CAM-B3LYP). Chem. Phys. Lett 2004, 393, 51–57.

(71). Chai J-D; Head-Gordon M Long-range corrected hybrid density functionals with damped atom-atom dispersion corrections. Phys. Chem. Chem. Phys 2008, 10, 6615–6620. [PubMed: 18989472]

(72). Becke AD Density-functional exchange-energy approximation with correct asymptotic behavior. Phys. Rev. A 1988, 38, 3098–3100.

(73). Becke AD A new mixing of Hartree-Fock and local densityfunctional theories. J. Chem. Phys 1993, 98, 1372.

(74). Lee C; Yang W; Parr RG Development of the Colle-Salvetti correlation-energy formula into a functional of the electron density. Phys. Rev. B 1988, 37, 785–789.

(75). Iikura H; Tsuneda T; Yanai T; Hirao K A long-range correction scheme for generalized-gradient-approximation exchange functionals. J. Chem. Phys 2001, 115, 3540–3544.

(76). Song J-W; Hirosawa T; Tsuneda T; Hirao K Long-range corrected density functional calculations of chemical reactions: Redetermination of parameter. J. Chem. Phys 2007, 126, 154105. [PubMed: 17461612]

(77). Vosko SH; Wilk L; Nusair M Accurate Spin-Dependent Electron Liquid Correlation Energies for Local Spin-Density Calculations - a Critical Analysis. Can. J. Phys 1980, 58, 1200–1211.

(78). Perdew JP Density-functional approximation for the correlation energy of the inhomogeneous electron gas. Phys. Rev. B 1986, 33, 8822–8824.

(79). Becke AD Density-functional exchange-energy approximation with correct asymptotic behavior. Phys. Rev. A 1988, 38, 3098–3100.

(80). Zhao Y; Truhlar DG Density Functional for Spectroscopy: No Long-Range Self-Interaction Error, Good Performance for Rydberg and Charge-Transfer States, and Better Performance on Average than B3LYP for Ground States. J. Phys. Chem. A 2006, 110, 13126–13130. [PubMed: 17149824]

(81). Chai J-D; Head-Gordon M Systematic optimization of long-range corrected hybrid density functionals. J. Chem. Phys 2008, 128, 084106. [PubMed: 18315032]

(82). Rohrdanz MA; Martins KM; Herbert JM A long-range-corrected density functional that performs well for both ground-state properties and time-dependent density functional theory excitation energies, including charge-transfer excited states. J. Chem. Phys 2009, 130, 054112. [PubMed: 19206963]

(83). Olsen J; Jørgensen P Linear and nonlinear response functions for an exact state and for an MCSCF state. J. Chem. Phys 1985, 82, 3235–3264.

(84). Hansen AE; Voigt B; Rettrup S Calculations of Chiroptical Properties of Organic Molecules: Program RPAC. Int. J. Quantum Chem. 1983, 23, 595–611.

(85). Bene JED; Ditchfield R; Pople JA Self-Consistent Molecular Orbital Methods. X. Molecular Orbital Studies of Excited States with Minimal and Extended Basis Sets. J. Chem. Phys 1971, 55, 2236.

(86). Foreman JB; Head-Gordon M; Pople JA; Frisch MJ Toward a Systematic Molecular Orbital Theory for Excited States. J. Phys. Chem 1992, 96, 135–149.

(87). Olsen J; Roos BO; Jørgensen P; Jensen HJA Determinant Based Configuration-Interaction Algorithms for Complete and Restricted Configuration-Interaction Spaces. J. Chem. Phys 1988, 89, 2185–2192.

(88). Perdew JP; Burke K; Ernzerhof M Generalized Gradient Approximation Made Simple. Phys. Rev. Lett 1996, 77, 3865–3868. [PubMed: 10062328]

(89). Perdew JP; Burke K; Ernzerhof M Generalized Gradient Approximation Made Simple – Errata. Phys. Rev. Lett 1996 , 78, 1396.

(90). Peverati R; Truhlar DG M11-L: A Local Density Functional That Provides Improved Accuracy for Electronic Structure Calculations in Chemistry and Physics. J. Phys. Chem. Lett 2012, 3, 117–124.

(91). Adamo C; Barone V Toward reliable density functional methods without adjustable parameters: The PBE0 model. J. Chem. Phys 1999, 110, 6158.

(92). Becke AD A new mixing of Hartree-Fock and local density-functional theories. J. Chem. Phys 1993, 98, 1372–1377.

(93). Zhao Y; Truhlar DG The M06 suite of density functionals for main group thermochemistry, thermochemical kinetics, noncovalent interactions, excited states, and transition elements: two new functionals and systematic testing of four M06-class functionals and 12 other function. Theor. Chem. Acc 2007, 120, 215–241.

(94). Henderson TM; Janesko BG; Scuseria GE Generalized gradient approximation model exchange holes for range-separated hybrids. J. Chem. Phys 2008, 128, 194105. [PubMed: 18500854]

(95). Baer R; Neuhauser D Density Functional Theory with Correct Long-Range Asymptotic Behavior. Phys. Rev. Lett 2005 , 94 , 043002. [PubMed: 15783554]

(96). Livshits E; Baer R A well-tempered density functional theory of electrons in molecules. Phys. Chem. Chem. Phys 2007, 9, 2932–2941. [PubMed: 17551616]

(97). Peverati R; Truhlar DG Improving the Accuracy of Hybrid Meta-GGA Density Functionals by Range Separation. J. Phys. Chem. Lett 2011, 2, 2810–2817.

(98). Casida ME; Jamorski C; Casida KC; Salahub DR Molecular excitation energies to high-lying bound states from time-dependent density-functional response theory: Characterization and correction of the time-dependent local density approximation ionization threshold. J. Chem. Phys 1998, 108, 4439–4449.

(99). Jacquemin D; Perpte EA; Ciofini I; Adamo C; Valero R; Zhao Y; Truhlar DG On the Performances of the M06 Family of Density Functionals for Electronic Excitation Energies. J. Chem. Theory Comput. 2010, 6, 2071–2085. [PubMed: 26615935]

(100). Schafer A; Horn H; Ahlrichs R Fully optimized contracted Gaussian basis sets for atoms Li to Kr. J. Chem. Phys 1992, 97, 2571.

(101). Ahlrichs R; Bar M; Marco H; Horn H; Kalmel C Electronic Structure Calculations on Workstation Computers: The Progam System TURBOMOLE. Chem. Phys. Lett 1989, 162, 165–169.

(102). Furche F; Ahlrichs R; Håttig C; Klopper W; Sierka M; Weigend F Turbomole. WIREs Comput. Mol. Sci. 2013, 4, 91–100.

(103). Shao Y; Fusti-Molnar L; Jung Y; Kussmann J; Ochsenfeld C; Brown ST; Gilbert ATB; Slipchenko LV; Levchenko SV; O'Neill DP et al. Advances in methods and algorithms in a modern quantum chemistry program package. Phys. Chem. Chem. Phys 2006, 8, 3172–91. [PubMed: 16902710]

(104). Krylov AI; Gill PM Q-Chem: an engine for innovation. WIREs Comput. Mol. Sci. 2013, 3, 317–326.

(105). Weigend F; Ahlrichs R Balanced basis sets of split valence, triple zeta valence and quadruple zeta valence quality for H to Rn: Design and assessment of accuracy. Phys. Chem. Chem. Phys 2005, 7, 3297–3305. [PubMed: 16240044]

(106). Rappoport D; Furche F Property-optimized gaussian basis sets for molecular response calculations. J. Chem. Phys 2010, 133, 134105. [PubMed: 20942521]

(107). Dunning TH Jr Gaussian basis sets for use in correlated molecular calculations. I. The atoms boron through neon and hydrogen. J. Chem. Phys 1989, 90, 1007–1023.

(108). Humphrey W; Dalke A; Schulten K VMD: Visual Molecular Dynamics. J. Mol. Graph 1996, 14, 33–38. [PubMed: 8744570]

(109). Suomivuori C-M; Lang L; Sundholm D; Gamiz-Hernandez AP; Kaila VRI Tuning the Protein-Induced Absorption Shifts of Retinal in Engineered Rhodopsin Mimics. Chem. Eur. J 2016, 22, 8254–8261. [PubMed: 27120137]

(110). Wang W; Nossoni Z; Berbasova T; Watson CT; Yapici I; Lee KSS; Vasileiou C; Geiger JH; Borhan B Tuning the electronic absorption of protein-embedded all-trans-retinal. Science 2012, 338, 1340–1343. [PubMed: 23224553]

(111). Grimme S; Antony J; Ehrlich S; Krieg H A consistent and accurate ab initio parametrization of density functional dispersion correction (DFT-D) for the 94 elements H-Pu. J. Chem. Phys 2010, 132, 154104. [PubMed: 20423165]

(112). Klamt A; Schüürmann G COSMO: a new approach to dielectric screening in solvents with explicit expressions for the screening energy and its gradient. J. Chem. Soc., Perkin Trans. 2 1993, 799–805.

(113). Wheeler SE; Houk KN Integration Grid Errors for Meta-GGA-Predicted Reaction Energies: Origin of Grid Errors for the M06 Suite of Functionals. J. Chem. Theory Comput. 2010, 6, 395–404. [PubMed: 20305831]

(114). Becke AD A multicenter numerical integration scheme for polyatomic molecules. J. Chem. Phys 1988, 88, 2547.

(115). Gill PMW; Johnson BG; Pople JA A standard grid for density functional calculations. Chem. Phys. Lett 1993, 209, 506–512.

(116). Baer R; Livshits E; Salzner U Tuned range-separated hybrids in density functional theory. Ann. Rev. Phys. Chem 2010, 61, 85–109. [PubMed: 20055678]

(117). Chantzis A; Laurent AD; Adamo C; Jacquemin D Is the Tamm-Dancoff Approximation Reliable for the Calculation of Absorption and Fluorescence Band Shapes? J. Chem. Theory Comput 2013, 9, 4517. [PubMed: 26589168]

(118). Grimme S A simplified Tamm-Dancoff density functional approach for the electronic excitation spectra of very large molecules. J. Chem. Phys 2013, 138, 244104. [PubMed: 23822224]

(119). Risthaus T; Hansen A; Grimme S Excited states using the simplified Tamm-Dancoff-Approach for range-separated hybrid density functionals: development and application. Phys. Chem. Chem. Phys 2014, 16, 14408–14419. [PubMed: 24356212]

(120). Li SL; Marenich AV; Xu X; Truhlar DG Configuration Interaction-Corrected Tamm-Dancoff Approximation: A Time-Dependent Density Functional Method with the Correct Dimensionality of Conical Intersections. J. Phys. Chem. Lett 2014, 5, 322–328. [PubMed: 26270707]

(121). Serrano-Andres L; Merchan M; Nebot-Gil I; Roos BO; Fulscher M Theoretical study of the electronic spectra of cyclopentadiene, pyrrole, and furan. J. Am. Chem. Soc 1993, 115, 6184–6197.

(122). Head-Gordon M; Grana AM; Maurice D; White CA Analysis of Electronic Transitions as the Difference of Electron Attachment and Detachment Densities. J. Phys. Chem 1995, 99, 14261–14270.

(123). Schreiber M; Silva-Junior MR; Sauer SPA; Thiel W Benchmarks for electronically excited states: CASPT2, CC2, CCSD, and CC3. J. Chem. Phys 2008, 128, 134110. [PubMed: 18397056]

(124). Winter NOC; Graf NK; Leutwyler S; Hattig C Benchmarks for 0-0 transitions of aromatic organic molecules: DFT/B3LYP, ADC(2), CC2, SOS-CC2 and SCS-CC2 compared to high-resolution gas-phase data. Phys. Chem. Chem. Phys 2013, 15, 6623–6630. [PubMed: 23111753]

(125). Sauer SPA; Schreiber M; Silva-Junior MR; Thiel W Benchmarks for Electronically Excited States: A Comparison of Noniterative and Iterative Triples Corrections in Linear Response Coupled Cluster Methods: CCSDR(3) versus CC3. J. Chem. Theory Comput. 2009, 5, 555–564. [PubMed: 26610222]

(126). Kánnár D; Szalay PG Benchmarking Coupled Cluster Methods on Valence Singlet Excited States. J. Chem. Theory Comput. 2014, 10, 3757–3765. [PubMed: 26588520]

(127). Jankowiak HC; Stuber JL; Berger R Vibronic transitions in large molecular systems: Rigorous prescreening conditions for Franck-Condon factors. J. Chem. Phys 2007, 127, 234101. [PubMed: 18154369]

(128). Koppel H; Domcke W; Cederbaum LS Multimode Molecular-Dynamics Beyond The Born-Oppenheimer Approximation. Adv. Chem. Phys 1984, 57, 59–246.

(129). Kallay M; Gauss J Calculation of excited-state properties using general coupled-cluster and configuration-interaction models. J. Chem. Phys 2004, 121, 9257–9269. [PubMed: 15538846]

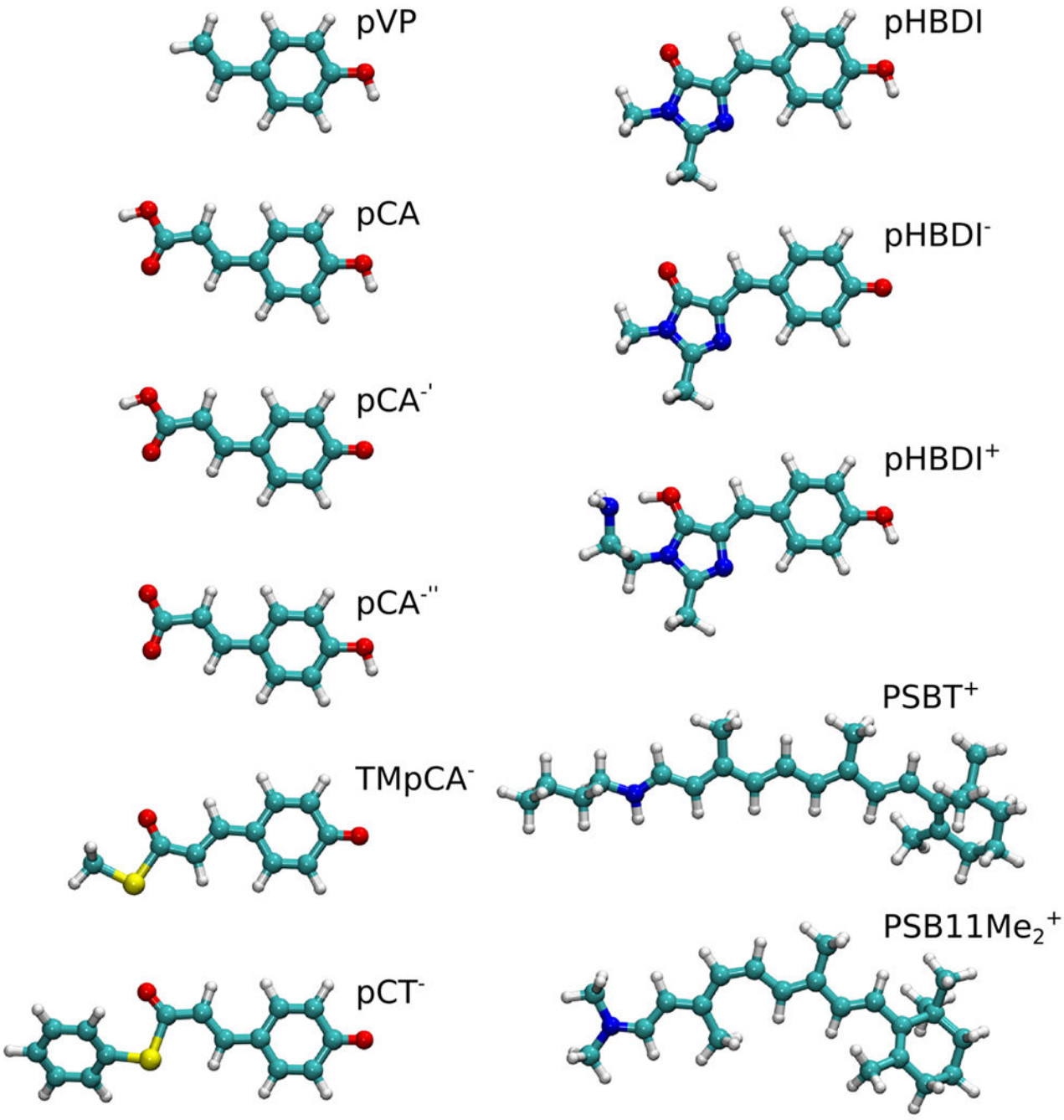

Figure 1:
The molecular structures of the studied biochromophores optimized at the B3LYP/def2-SVP level of theory. The figure was prepared using VMD.[108]

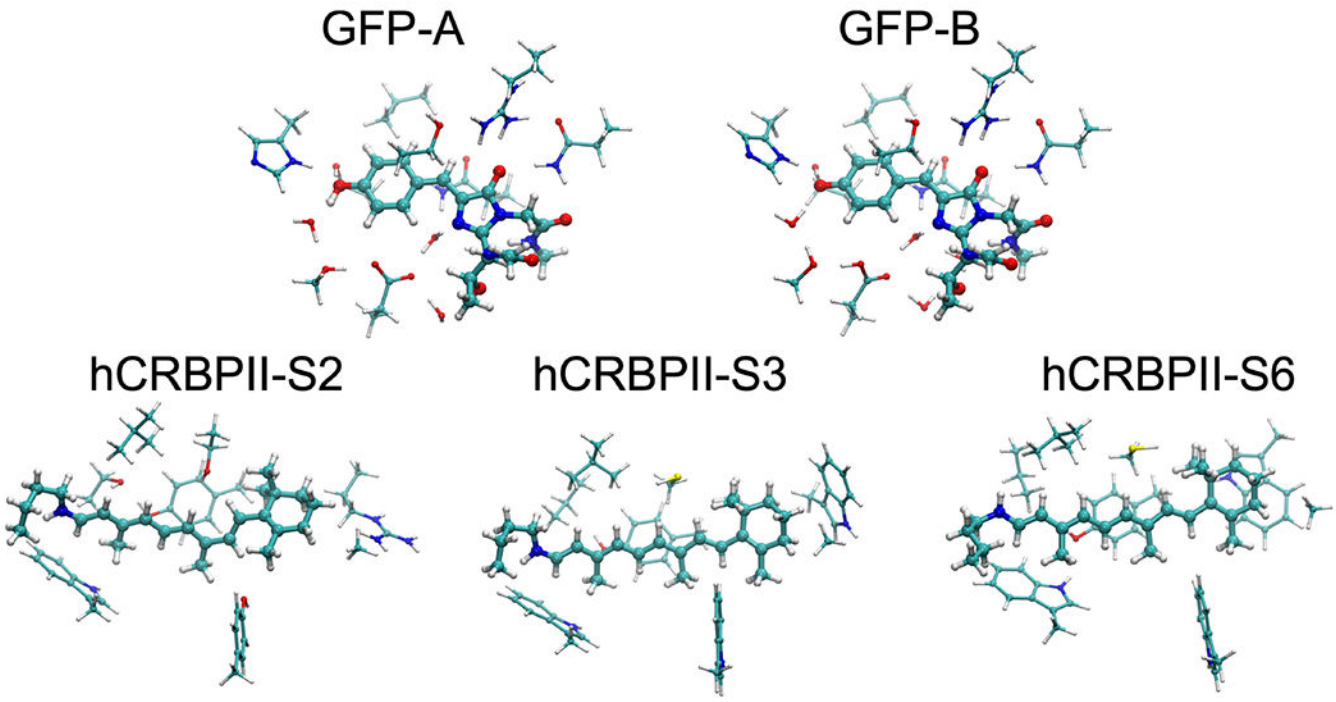

Figure 2:
The molecular structures of the studied protein models. The figure was prepared using VMD.[108]

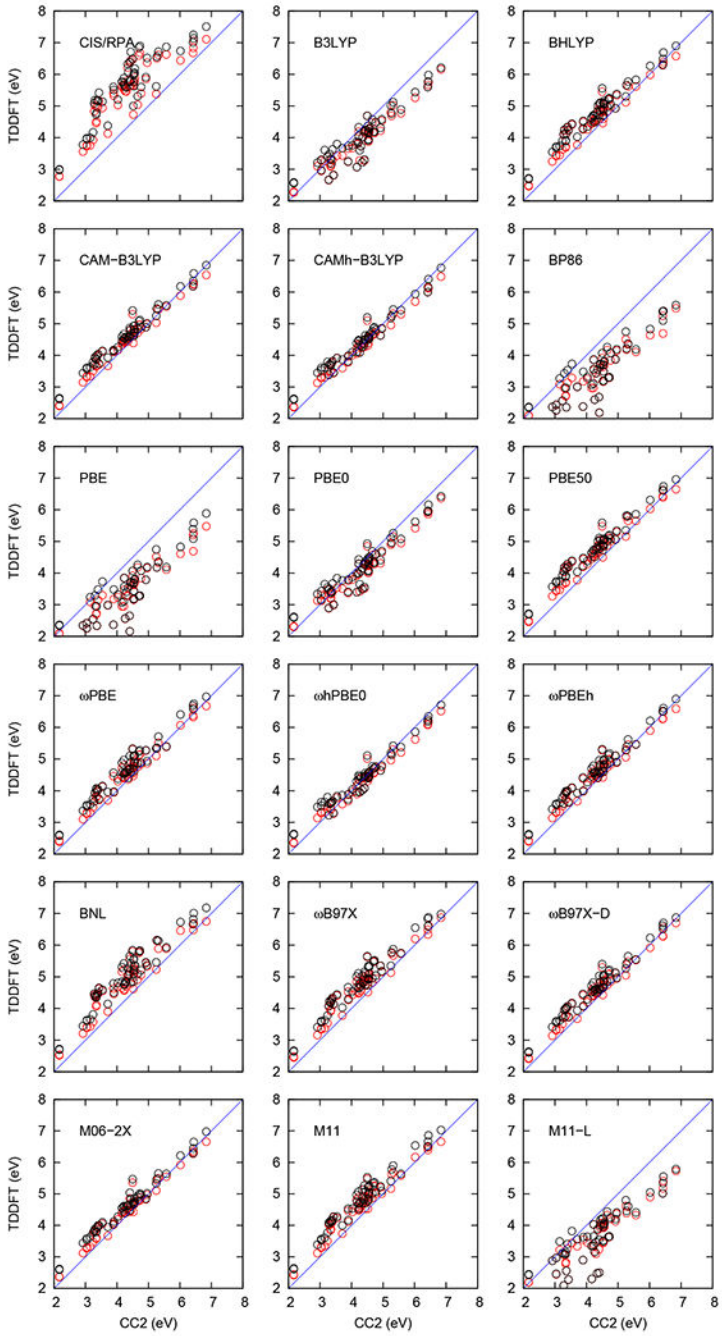

Figure 3:

The performance of TDDFT functionals as compared with CC2 excitation energies calculated using def2-TZVP basis sets. The VEEs (in eV) calculated using TDDFT and TDA method are shown in red and black, respectively.

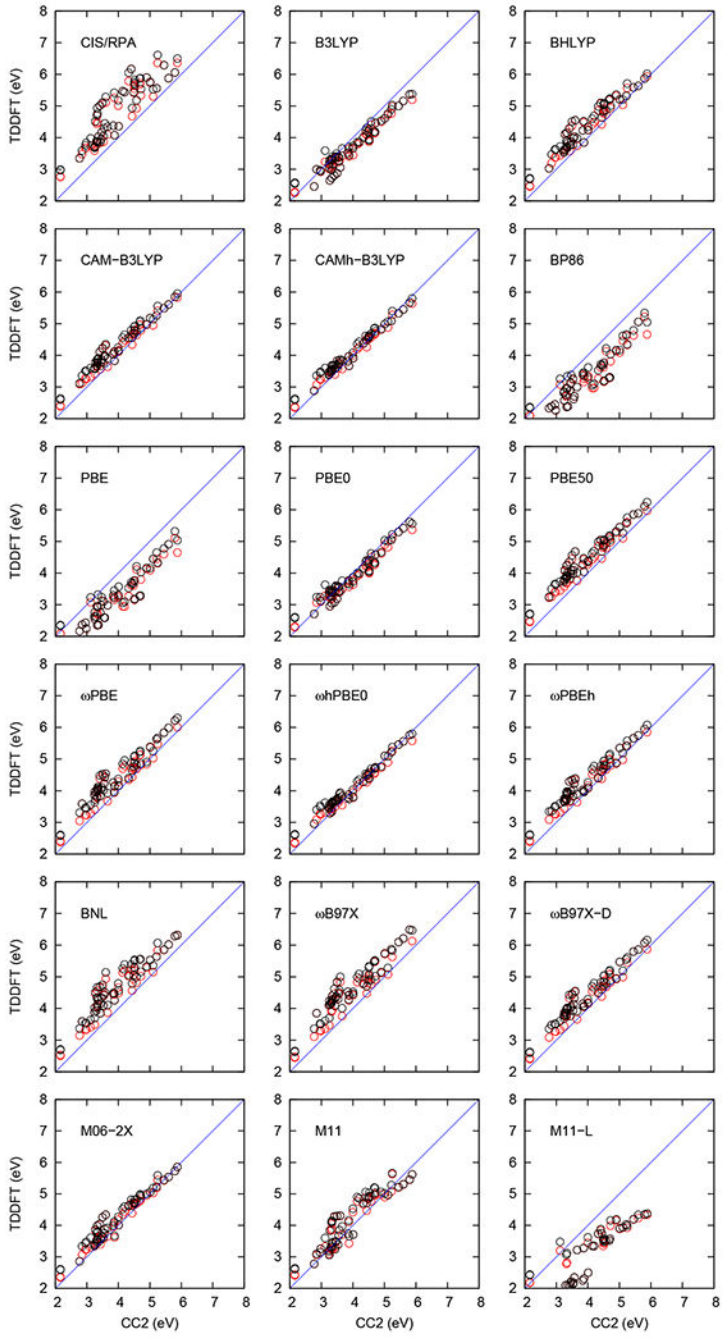

Figure 4:

The performance of TDDFT functionals as compared with CC2 excitation energies calculated using aug-def2-TZVP basis sets. The VEEs (in eV) calculated using TDDFT and TDA method are shown in red and black, respectively.

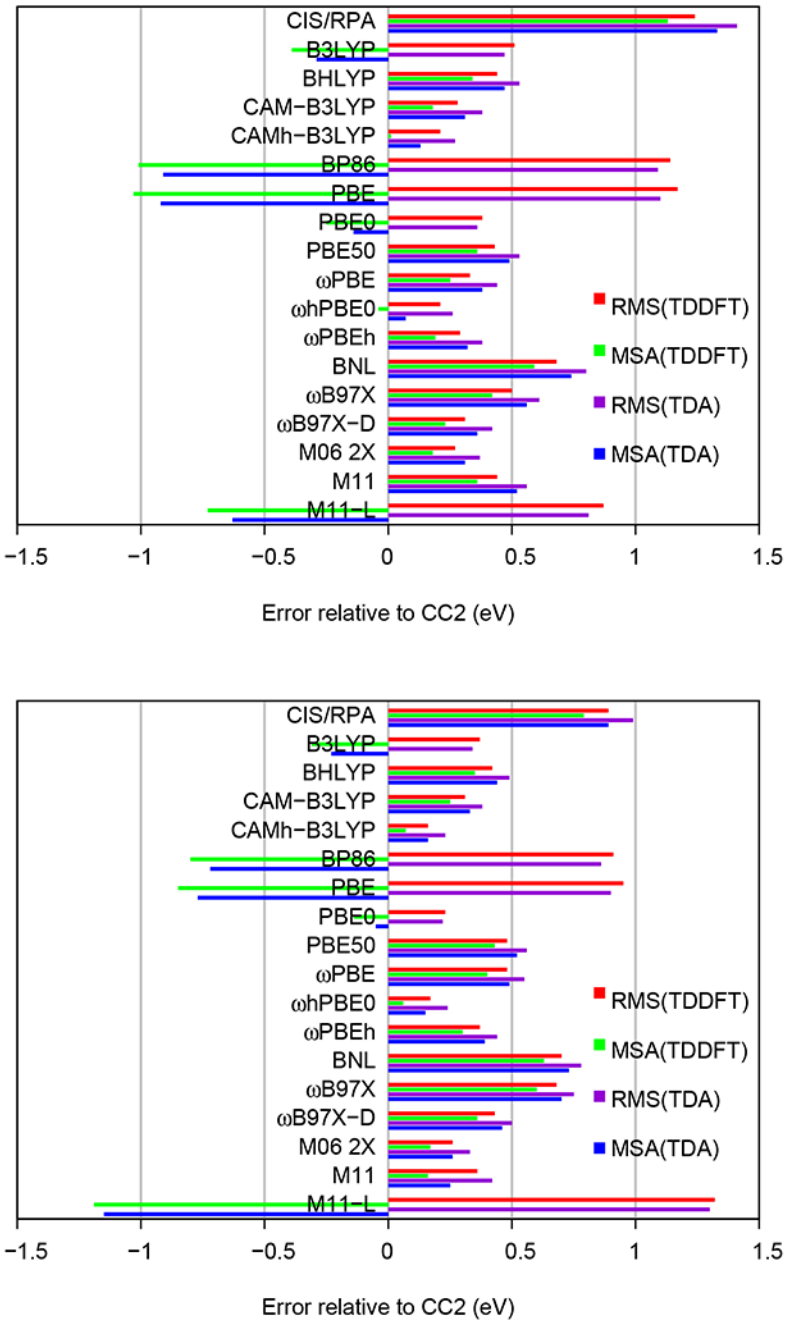

Figure 5:

The root-mean-square (RMS) and mean signed average (MSA) differences (in eV) between VEEs calculated at the TDDFT, TDA and CC2 levels using the def2-TZVP basis sets (top panel) and aug-def2-TZVP basis sets (bottom panel). The excitation energies of the five lowest excited state of the 11 chromophores are included.

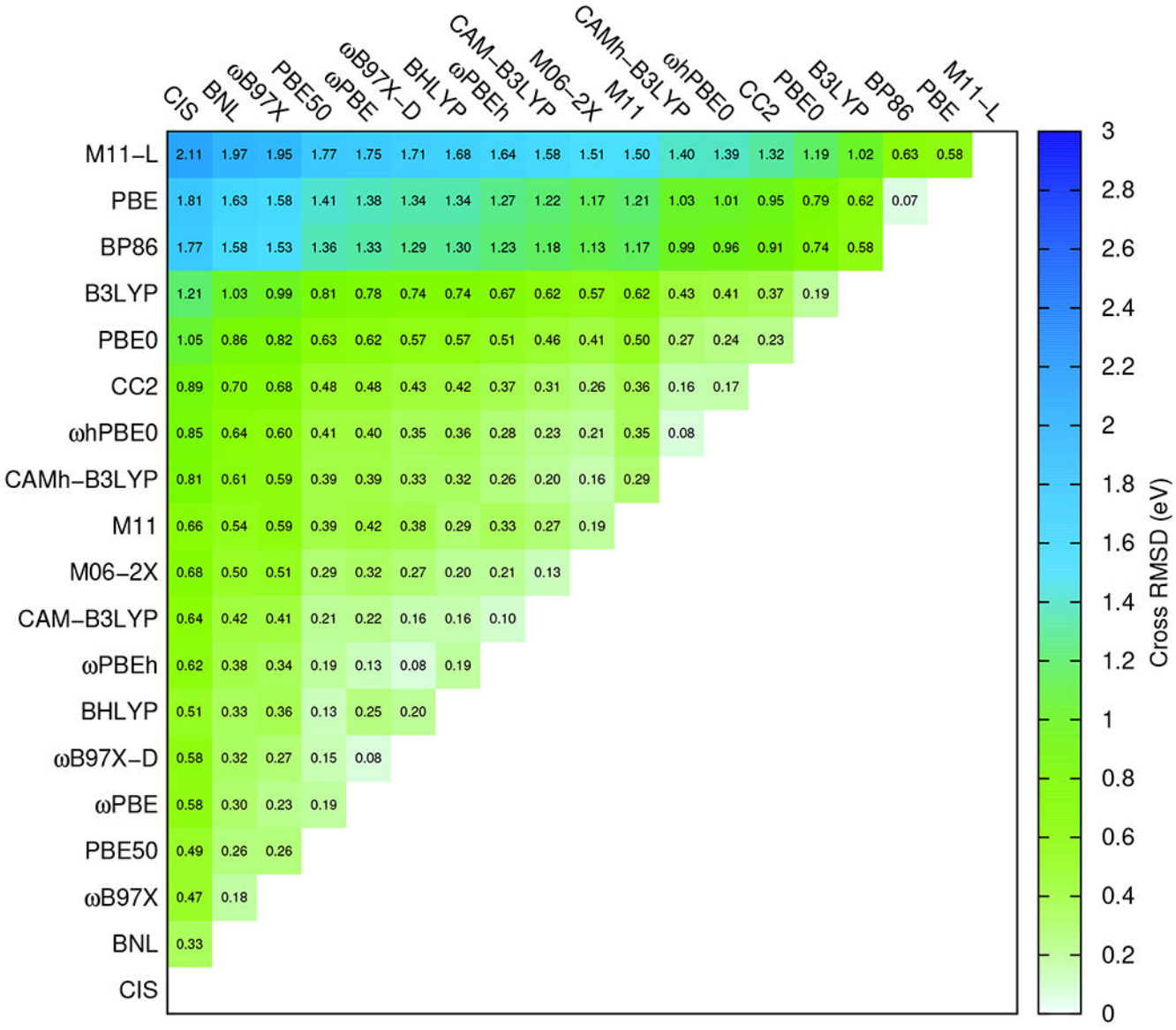

Figure 6:

Cross-RMS values calculated for VEEs at the TDDFT level using different functionals obtained and the aug-def2-TZVP basis sets.

Table 1:

The amount of short-range and long-range HF exchange in the 17 studied DFT functionals. C_{HF}^{sr} and C_{HF}^{sr} is the amount of HF exchange in the short-range (sr) and long-range (lr) regime, respectively. The ω values of the error function of the range-separated functionals are also given.

Functional	Reference	C_{HF}^{sr}	C_{HF}^{lr}	ω
CIS/RPA	84–86	1.0	1.0	-
B3LYP	72–74	0.2	-	-
BHLYP	92	0.5	-	-
CAM-B3LYP	70	0.19	0.65	0.33
CAMh-B3LYP	this work	0.19	0.50	0.33
BP86	77–79	0	-	-
PBE	88,89	0	-	-
PBE0	91	0.25	-	-
PBE50	88,89,91	0.5	-	-
ωPBE	82,94	0	1.0	x.z
ωhPBE0	this work	0.25	0.50	x.s
ωPBEh	82	0.20	1.0	x.d
ωB97X	81	0.157706	1.0	x.d
ωB97X-D	71	0.222036	1.0	x.d
BNL	95,96	0	1.0	-
M06-2X	93	0.54	-	-
M11	97	0.428	1.0	-
M11-L	90	0	-	-

Table 2:

Excitation energies (in eV) for DFT-optimized protein models of the green fluorescent protein (GFP) and the retinoid-binding protein II (hCRBPII) calculated at the CC2 and TDDFT levels using a few selected functionals. The calculations were performed with def2-TZVP basis sets.

Model/Method	CC2	B3LYP	CAM-B3LYP	CAMh-B3LYP	Exp.
GFP-A[a]	3.13	2.98	3.70	3.14	3.12
GFP-B[a]	2.72	2.91	2.79	2.76	2.61
hCRBPII-S2[b]	2.37	1.78	2.60	2.51	2.44
hCRBPII-S3[b]	2.13	1.45	2.42	2.39	2.10
hCRBPII-S6[b]	2.03	1.26	2.34	2.31	1.99

[a] CC2 data and protein model from Refs 10 and 11.

[b] CC2 data and protein model from Ref. 109.